International Journal of Recent Research and Review, Vol. XIX, Issue 3, September 2026

ISSN 2277 – 8322

STOCKWELL TRANSFORM-BASED FAULT DETECTİON AND CLASSİFİCATİON İN RENEWABLE ENERGY-INTEGRATED DİSTRİBUTİON POWER SYSTEMS

[1] Khem Raj Mahawar, [2]Dr. Bharat Bhushan Jain

[1]M.Tech Student, Department of Electrical Engineering, Jaipur Engineering College, Jaipur

k.rjmahawar@gmail.com

[2]Professor, Department of Electrical Engineering, Jaipur Engineering College, RTU Kota

drbharatjainjec@gmail.com

Abstract: The increasing integration of distributed generation (DG), particularly renewable energy sources such as solar and wind energy, has significantly changed the operating characteristics and fault behavior of modern distribution power systems. These changes can affect the performance of conventional protection equipment and make the rapid detection and classification of symmetrical and unsymmetrical faults more challenging. Therefore, reliable and efficient fault-detection techniques are essential for maintaining the stability, security, and continuity of power supply. This paper proposes a Stockwell Transform (ST)-based approach for the detection and classification of faults in renewable energy-integrated distribution power systems. The proposed method utilizes the time-frequency characteristics of electrical signals obtained through the Stockwell Transform to construct an S-matrix-based fault index. Appropriate threshold values and a decision algorithm are employed to distinguish normal operating conditions from fault conditions and to identify different fault types. The proposed approach is implemented and evaluated on an IEEE 33-bus distribution system using MATLAB/Simulink under renewable-energy-integrated operating conditions. The results demonstrate the capability of the Stockwell Transform to effectively extract fault-related signal characteristics and provide rapid and reliable identification of symmetrical and unsymmetrical faults. The proposed method offers a promising approach for enhancing fault protection and monitoring in modern distribution networks with renewable energy integration.

Keywords: Stockwell Transform; Fault Detection; Fault Classification; Renewable Energy; Distributed Generation;

ISSN 2277 – 8322

Distribution Power System; S-Matrix; Fault Index; Symmetrical Faults; Unsymmetrical Faults.

I. INTRODUCTION

In Faults are unavoidable in modern electrical and power systems and can significantly affect the efficiency, reliability, and safety of power networks. Fault conditions may arise due to equipment failure, insulation deterioration, conductor damage, environmental disturbances, component aging, external interference, or sudden changes in electrical signals [1]. If faults are not detected and cleared rapidly, they can result in equipment damage, voltage instability, interruption of power supply, and, in severe cases, widespread blackouts. Therefore, accurate and rapid fault detection, classification, and location are essential for maintaining the reliability and continuity of electrical power systems. Fault diagnosis in power systems involves the detection of abnormal operating conditions, identification of the fault type, and estimation of the fault location. In transmission and distribution networks, common fault conditions include Single Line-to-Ground (LG) Fault, Line-to-Line (LL) Fault, Double Line-to-Ground (LLG) Fault, Three-Phase-to-Ground (LLLG) Fault. Accurate identification of these faults enables protection systems to isolate the affected section quickly and supports faster maintenance and restoration of the power supply.

Several signal-processing and intelligent techniques have been developed for power-system fault detection and classification. Conventional approaches are generally based on electrical quantities such as voltage, current, impedance, and phase-angle variations. However, the nonlinear and transient nature of fault signals has encouraged the use of advanced signal-processing techniques such as WT, Fourier Transform, Stockwell Transform (S-transform), fuzzy logic, ANNs and other machine learning approaches [2]. These techniques can extract useful time-frequency features from transient voltage and current signals and improve the reliability of fault identification. A detailed review of intelligent techniques for fault diagnosis in electric power transmission systems was reported in [3], emphasizing the increasing application of intelligent methods for reliable fault detection and diagnosis. In [4], a fault-location technique for multi-terminal transmission lines was developed using unsynchronized measurements. The proposed method incorporated a synchronization procedure to accurately

ISSN 2277 – 8322

estimate the fault location while minimizing the effects of variations in fault resistance and source impedance. Its effectiveness was evaluated under different fault conditions, including high fault-resistance scenarios. The results indicated that the method provided fast and reliable fault-location performance and showed good robustness against transient disturbances in the power system.

Wavelet Transform-based techniques have also been extensively investigated for monitoring, detecting, classifying, and locating faults in transmission lines [5]. In such approaches, voltage and current signals measured at different locations of the transmission line are analyzed using wavelet-based coefficients or energy-related indices. In some systems, GPS synchronization is employed to synchronize measurements obtained from both ends of a transmission line. Fault indices derived from current or voltage signals are compared with predefined threshold values to identify abnormal conditions. Artificial Neural Networks have also been applied for fault classification and location by using extracted features from the approximate and detailed components of voltage and current signals.

The increasing penetration of Distributed Generation (DG) has introduced additional challenges in power-system protection and fault diagnosis. DG refers to small- or medium-scale generation units connected close to electrical loads within distribution networks. Renewable energy sources such as solar photovoltaic and wind energy are among the major forms of DG. Although DG improves energy efficiency, reduces transmission losses, and supports the integration of renewable energy, its presence changes the magnitude and direction of fault currents and modifies the overall behavior of distribution networks. Consequently, conventional protection systems may experience difficulties in detecting and discriminating faults accurately. The number, location, and operating conditions of DG units can vary significantly, resulting in changing fault-current characteristics and protection requirements. The introduction of DG can therefore affect the coordination and operating characteristics of protective devices in distribution networks [6]. These challenges highlight the need for advanced fault-detection and classification techniques capable of operating reliably under varying network configurations and renewable-energy penetration levels.

ISSN 2277 – 8322

II. PROPOSED METHODOLOGY

Distribution The proposed method for power transmission line safety involves fault detection using approach of fault index. For fault detection, the ST matrix is used. In the subsections that follow, we'll go over how to calculate fault index and a quick overview of the Stockwell transform.

2.1 Fault Transform Index

To distinguish between the defective and healthy stages, a fault index is suggested. On the EHV transmission line, this index is often used to distinguish between different faults. The following measures are used to measure the fault index:

- The current of all phases is recorded on the test system's bus 800.
- Current signals are disintegrated using the Stockwell Transform at a sampling rate of 20 kHz, yielding an S-matrix.
- The S-median matrix's is found.
- The perfect value of the median is estimated and the fault index is assigned.
- The fault indices is used to locate and detect faults

2.2 Stockwell

STFT of the signal c(t) is defined by the following relation.

$$\mathrm{STFT}(\tau, f) = \int_{-\infty}^{+\infty} c(t)h(\tau - t)e^{-j2\pi ft}dt \quad (1)$$

where spectral localization time and Fourier frequency are denoted by and f, respectively, and g(t) is a window function. The S transform can be derived from the above equation by substituting the Gaussian function for the window functiong(t).

$$.h(t) = \frac{|f|}{\sqrt{2\pi}} e^{-\frac{f^2 t^2}{2}} \quad (2)$$

Hence,

$$S(\tau, f) = \int_{-\infty}^{+\infty} c(t)\frac{|f|}{\sqrt{2\pi}} e^{\frac{f^2(\tau-t)^2}{2}} e^{-j2\pi ft}dt \quad (3)$$

The S transform is thus a variant of the STFT with a Gaussian window function. If the time domain window of the S-transform is larger, it can results higher frequency resolution for lower frequencies. Even though the window is smaller, it can results improved time resolution for higher frequencies. The S-transform produces an S-matrix, which is a matrix. The S-matrix can be used to extract knowledge about the signal's frequency and amplitude.

III. PROPOSED TEST SYSTEM

The proposed. system is a typical IEEE-33 bus test system. All of the feeders used

ISSN 2277 – 8322

in the test system are three step, with lengths equal to the feeders' original lengths. The loads in the test device are all 3 ϕ loads. Spot loads in the centre of the feeders are used to simulate distributed loads.

As shown in Fig. 1, the test system considered in this study is based on the IEEE 33-bus distribution system. The system consists of three-phase feeders, with the feeder lengths maintained according to the original IEEE test-system configuration. All loads in the test system are considered as three-phase loads. Spot loads are placed at appropriate locations along the feeders to represent the distributed loading conditions of the network. The detailed parameters of the test system, including transformer specifications, distributed load data, spot-load information, capacitor-bank ratings, and line-segment parameters, are presented in Tables 1–5, respectively. These parameters are used to develop and simulate the distribution network under different operating and fault conditions. For evaluating the proposed fault detection and classification method, different fault conditions are introduced at the specified location of the test system, as described in the simulation results section. The fault cases are analyzed to evaluate the effectiveness of the proposed methodology in detecting and classifying power system faults.

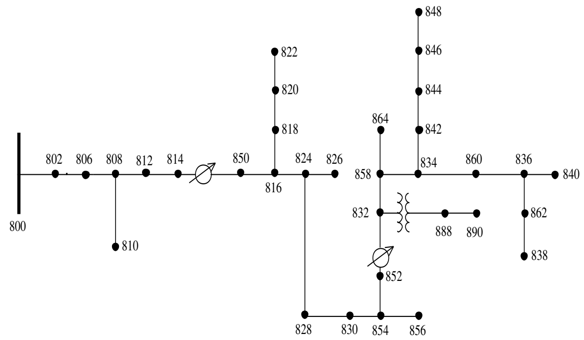

Fig 1: IEEE 33 Bus test system for fault analysis

Table 1: Phase Parameters For Distribution Network

S. No.	Node A	Node B	Load Model	Ph-1 KW	Ph-1 KVAr	Ph-2 KW	Ph-2 KVAr	Ph-3 KW	Ph-3 KVAr
01.	802	806	Y-PQ	0	0	30	15	25	14
02.	808	810	Y-I	0	0	16	8	0	0
03.	818	820	Y-Z	34	17	0	0	0	0
04.	820	822	Y-PQ	135	70	0	0	0	0
05.	816	824	D-I	0	0	5	2	0	0

06.	824	826	Y-I	0	0	40	20	0	0
07.	824	828	Y-PQ	0	0	0	0	4	2
08	828	830	Y-PQ	7	3	0	0	0	0
09.	854	856	Y-PQ	0	0	4	2	0	0
10.	832	858	D-Z	7	3	2	1	6	3
11.	858	864	Y-PQ	2	1	0	0	0	0
12.	858	834	D-PQ	4	2	15	8	13	7
13.	834	860	D-Z	16	8	20	10	110	55
14.	860	836	D-PQ	30	15	10	6	42	22
15.	836	840	D-I	18	9	22	11	0	0
16.	862	838	Y-PQ	0	0	28	14	0	0
17.	842	844	Y-PQ	9	5	0	0	0	0
18.	844	846	Y-PQ	0	0	25	12	20	11
19.	846	848	Y-PQ	0	0	23	11	0	0
Total				262	133	240	120	220	114

Table 2: % Resistance and % Reactances of Trasnformers

Transformer	**kVA**	**kV-high**	**kV-low**	**R (%)**	**X (%)**
Substation	2500	69 –D	24.9 –Gr.W	1	8
XFM-1	500	24.9 – Gr.W	4.16 –Gr.W	1.9	4.08

Table 3: Phase Parameters for Spot

S. No.	Node	Load Model	Ph-1 KW	Ph-1 KVAr	Ph-2 KW	Ph-2 KVAr	Ph-3 KW	Ph-4 KVAr
01.	860	Y-PQ	20	16	20	16	20	16
02.	840	Y-I	9	7	9	7	9	7
03.	844	Y-Z	135	105	135	105	135	105
04.	848	D-PQ	20	16	20	16	20	16
05.	890	D-I	150	75	150	75	150	75
06.	830	D-Z	10	5	10	5	25	10
	Total		344	224	344	224	359	229

Table 4: Capacitor phase parameters

Node	Ph-A (kVAr)	Ph-B (kVar)	Ph-C (kVAr)
844	100	100	100
848	150	150	150
Total	250	250	250

Fig. 2 depicts the proposed test method as modeled in MATLAB. This model also depicts the data collection system used in this analysis. The 3 ϕ Simulink block is used to model the feeders. Simulink three step load blocks are used to simulate the loads. Simulink 3 ϕ fault block is used to

ISSN 2277 – 8322

model power system faults. A generator block simulates the utility grid.

Table 5: Line Segment Parameters

S. No.	Node A	Node B	Length(ft.)	Config.
01	800	802	2580	300
02	802	806	1730	300
03	806	808	32230	300
04	808	810	5804	303
05	808	812	37500	300
06	812	814	29730	300
07	814	850	10	301
08	816	818	1710	302
09	816	824	10210	301
10	818	820	48150	302
11	820	822	13740	302
12	824	826	3030	303
13	824	828	840	301
14	828	830	20440	301
15	830	854	520	301
16	832	858	4900	301
17	832	888	0	XFM-1
18	834	860	2020	301
19	834	842	280	301
20	836	840	860	301
21	836	862	280	301
22	842	844	1350	301
23	844	846	3640	301
24	846	848	530	301
25	850	816	310	301
26	852	832	10	301
27	854	856	23330	303
28	854	852	36830	301
29	858	864	1620	302
30	858	834	5830	301

The simulation parameters of the proposed power system model are presented in Figs. 3–7. Fig. 3 shows the grid parameters used for the simulation, while Fig. 4 presents the parameters of the substation transformer. The simulation parameters of the power transmission line are illustrated in Fig. 5. The parameters of transformer XFM-1 connected in the Simulink model are shown in Fig. 6, and the parameters of the load connected to the Simulink model are presented in Fig. 7. These parameters define the major components and operating conditions of the test system used for the simulation and analysis.

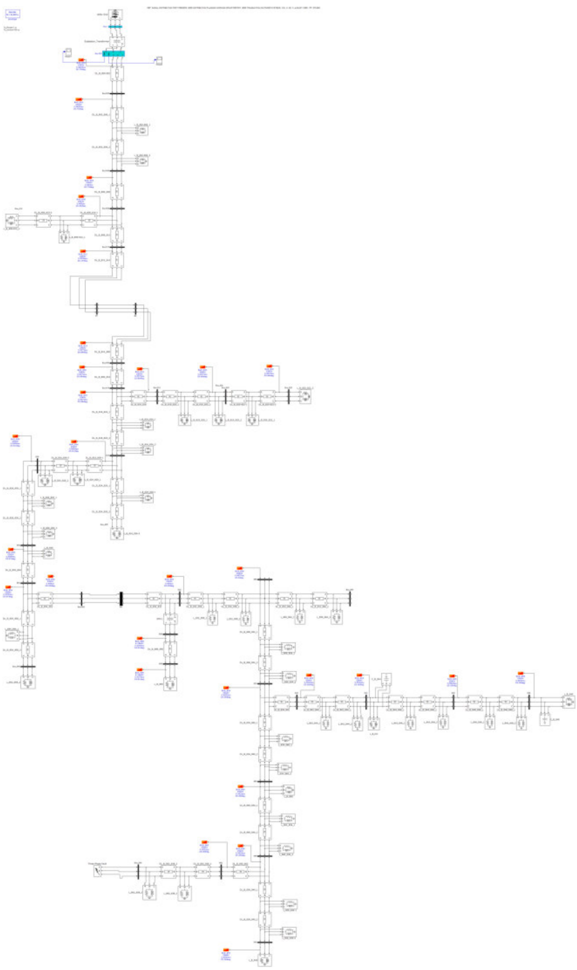

Fig 2: Simulink model for proposed IEEE 33 bus test system

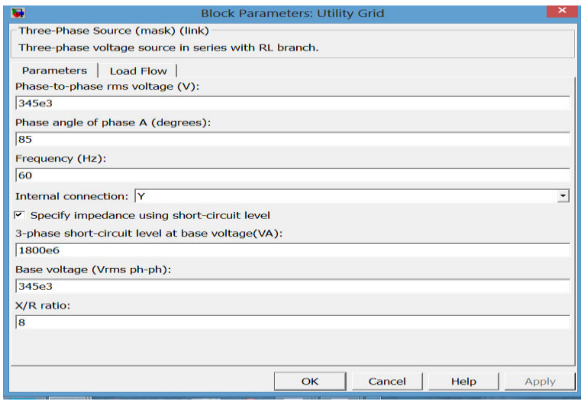

Fig 3: Grid Parameters for simulation

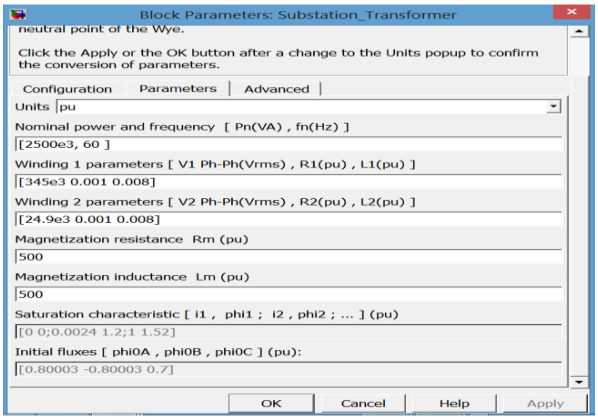

Fig 4: Simulation parameter for substation transformer

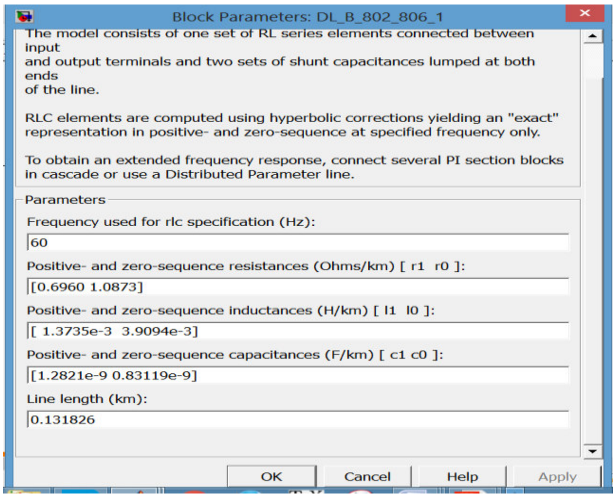

Fig 5: Simulation parameters of power transmission line

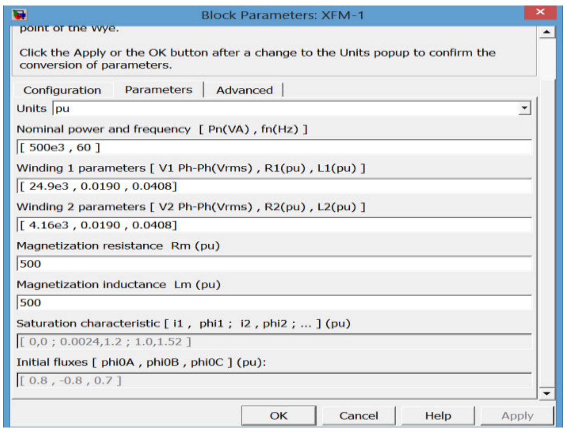

Fig 6: Simulation parameters of Transformer XFM-1connected in simulink model

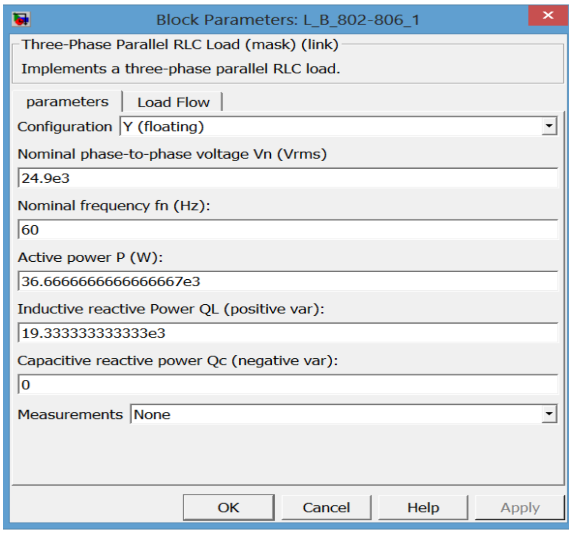

Fig 7: Simulation parameters for Load connected in simulink

IV. RESULTS & DISCUSSION

The complete IEEE 33 bus test system is evaluated with the two types of results; in first result current waveform is obtained and another one result fault index graph is obtained for symmetrical and unsymmetrical faults. Effect of various types of faults mentioned in subsections are evaluated and plotted at the 6 cycle of the simulation of 12 cycles.

4.1.Identification of Faults without Renewable Sources

The IEEE-33 bus test system shown in Fig. 1 is considered for the analysis. Different types of faults are introduced at Bus 838, and the corresponding three-phase current signals are recorded for analysis. Each simulation waveform consists of 12 cycles, with the fault initiated at the sixth cycle. Based on the analysis of 30 fault cases for each fault type, a threshold value of 10 is selected for the proposed fault index. The simulation results for different fault conditions are presented and discussed in the following sections.

A. Analysis of Line to Ground Fault

A LG fault is created by connecting Phase A to ground at Bus 838. The corresponding three-phase current waveforms are presented in Fig. 8. Before the occurrence of the fault, the three-phase currents remain within their normal operating range. When the fault is initiated at the sixth cycle, the magnitude of the Phase-A current increases significantly, from approximately 50 A to 300 A. In contrast, the currents in the healthy phases, Phases B and C, remain comparatively stable. This significant increase in the current of the faulted phase indicates the occurrence of an LG fault.

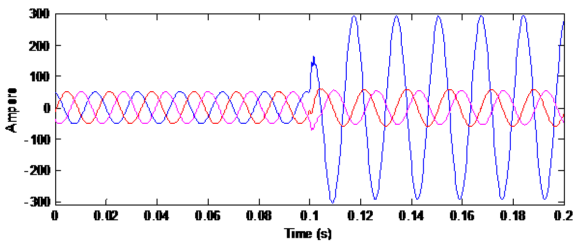

Fig. 8: Three-phase current waveforms during the line-to-ground fault at Bus 838

The corresponding fault index values obtained using the proposed Stockwell Transform-based method is shown in Fig. 9. The fault index of the faulted Phase A increases significantly and reaches a maximum value of approximately 13, which is higher than the selected threshold value of 10. In comparison, the fault index values of the healthy Phases B and C remain below the threshold. Therefore, the proposed fault index successfully detects the occurrence of the line-to-ground fault and identifies the faulted phase.

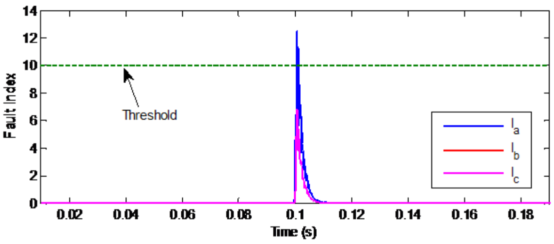

Fig. 9: Stockwell Transform-based fault index for the line-to-ground fault

B. Analysis of Double Line Fault

A LL fault is created by short-circuiting Phases A and B at Bus 838. The corresponding three-phase current waveforms during the LL fault are shown in Fig. 10. Before the fault occurrence, the phase currents remain at their normal operating levels. When the fault is initiated at the sixth cycle, the current magnitudes of Phases A and B increase significantly from approximately 50 A to 350 A. In comparison, the current magnitude of the healthy Phase C remains nearly unchanged. Thus, the fault results in a substantial increase in the currents of the two faulted phases, indicating the occurrence of an LL fault.

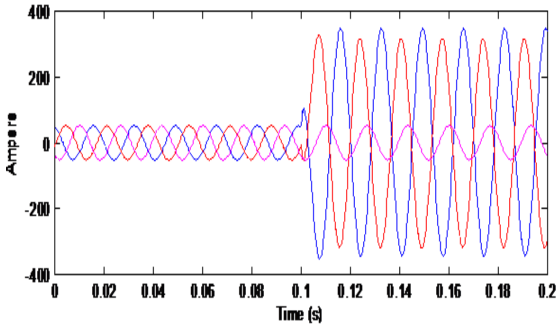

Fig. 10: Three-phase current waveforms during the double-line fault at Bus 838

The corresponding values of the proposed fault index for the three phases are presented in Fig. 11. The fault indices of the faulted Phases A and B increase significantly and reach a maximum value of approximately 16, which is higher than the predefined threshold value of 10. In contrast, the fault index of the healthy Phase C remains approximately zero and well below the threshold. Therefore, the proposed Stockwell Transform-based fault index successfully detects the LL fault and identifies Phases A and B as the faulted phases.

ISSN 2277 – 8322

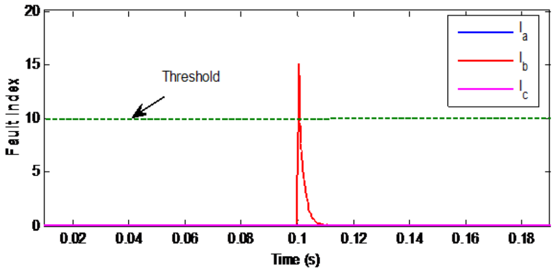

Fig. 11: Stockwell Transform-based fault index for the double-line fault at Bus 838

C. Analysis of Double Line to Ground Fault

A LLG fault is created by simultaneously connecting Phases A and B to ground at Bus 838. The corresponding three-phase current waveforms during the LLG fault are presented in Fig. 12. Before the fault occurrence, the phase currents remain within their normal operating range. When the fault is initiated, the current magnitudes of the faulted Phases A and B increase significantly. In comparison, the current in the healthy Phase C remains comparatively stable. The substantial increase in the currents of Phases A and B indicates the occurrence of a double-line-to-ground fault.

The corresponding fault index values obtained using the proposed Stockwell Transform-based method are shown in Fig. 13. The fault indices of Phases A and B reach a maximum value of approximately 16, which is higher than the predefined threshold value of 10.

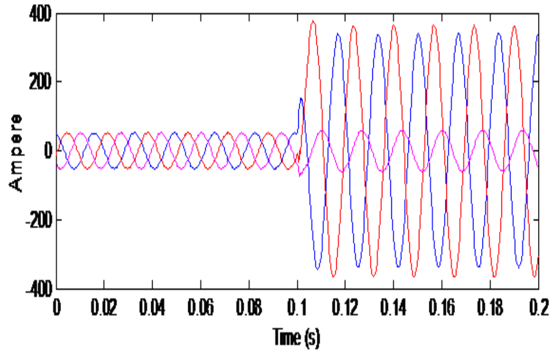

Fig. 12: Three-phase current waveforms during the double-line-to-ground fault at Bus 838

The fault index of the healthy Phase C is approximately 4, which remains below the threshold. Therefore, the proposed fault index successfully detects the occurrence of the LLG fault and identifies Phases A and B as the faulted phases.

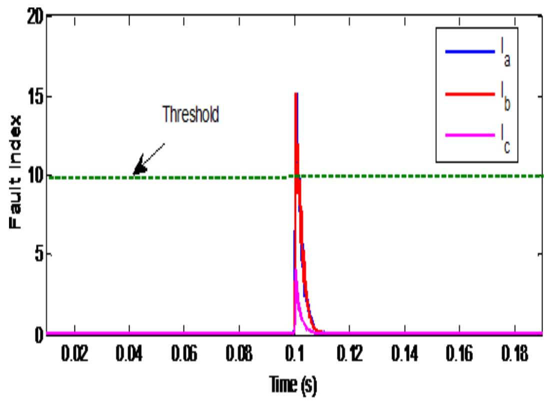

Fig. 13: Stockwell Transform-based fault index for the double-line-to-ground fault at Bus 838

D. Analysis of Three Phase Fault Involving Ground

A LLLG fault is created by simultaneously connecting Phases A, B, and C to ground at Bus 838. The corresponding three-phase current waveforms are presented in Fig. 14. Under normal operating conditions, the three-phase currents remain within their respective steady-state values. When the LLLG fault occurs, the current magnitude in all three phases increases significantly and reaches approximately 400 A. This considerable increase in current indicates the occurrence of a severe three-phase-to-ground fault.

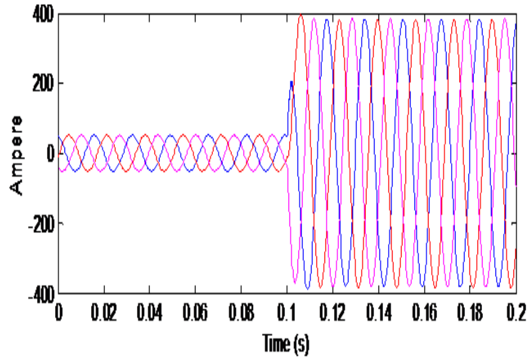

Fig. 14: Three-phase current waveforms during the three-phase-to-ground fault at Bus 838

The corresponding fault index values obtained using the proposed Stockwell Transform-based median approach are shown in Fig. 15. It is observed that the fault index values of all three phases increase significantly and exceed the predefined threshold value of 10. The fault index values are greater than 25, clearly indicating the presence of a fault in all three phases. Therefore, the proposed algorithm successfully detects and identifies the LLLG fault.

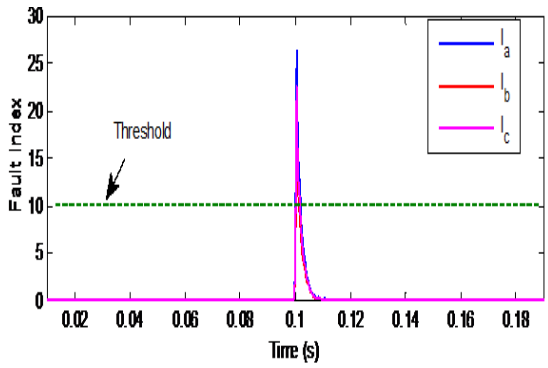

Fig. 15: Stockwell Transform-based fault index for the three-phase-to-ground fault at Bus 838

E. Comparative Study

The peak fault-index values obtained for the different fault conditions are presented in Table 6. The proposed fault index provides a clear distinction among the different types of power system faults based on the magnitude and distribution of the index values across the three phases.

The LLLG fault produces the highest fault-index values because all three phases are involved in the fault. The LG fault produces comparatively lower fault-index values, with only one phase being primarily affected. For the LL fault, the fault indices of the two faulted phases are significantly higher than those of the healthy phase. In the case of the LLG fault, the two faulted phases also exhibit high fault-index values, while the healthy phase shows a comparatively lower value. Therefore, the proposed fault index can effectively distinguish among LG, LL, LLG, and LLLG faults by analyzing the peak index values of the three phases.

Table 6: Peak Fault-Index Values For Different Fault Conditions at Bus 838

S. No.	Type of Fault	Phase-A	Phase-B	Phase-C
1	LG	13	7	7
2	LL	16	16	0
3	LLG	16	16	4
4	LLLG	27	24	24

4.2.Identification of Faults with Renewable Energy Penetration

A. Analysis of Line to Ground Fault

A LG fault is introduced on Phase A at Bus 838 in the presence of the wind energy conversion system. The corresponding three-phase current waveforms are presented in Fig. 16. Before the occurrence of the fault, the three-phase currents remain within their normal operating range. When the fault occurs at the 20th cycle, the current magnitude increases significantly, particularly in the faulted phase. The variation in the current waveform clearly indicates the occurrence of the LG fault under wind power penetration.

The corresponding variation in the proposed fault index is shown in Fig. 17. The fault index of the faulted Phase A increases to a value greater than 5, exceeding the selected threshold value of 4. In comparison, the fault-index values of the healthy phases remain below the threshold and reach approximately 2.5.

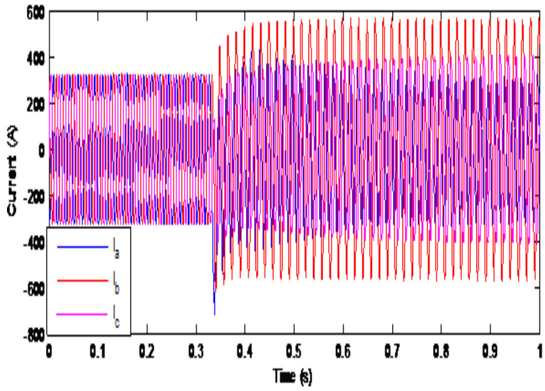

Fig. 16: Three-phase current waveforms during the LG fault in the presence of WECS

Therefore, the proposed fault index clearly distinguishes the faulted Phase A from the healthy phases in the presence of WECS. The results demonstrate that the proposed Stockwell Transform-based fault index remains effective for fault detection even after the integration of wind power generation into the distribution network. The fault index also exhibits a relatively rapid rise following fault inception, enabling timely identification of the fault condition.

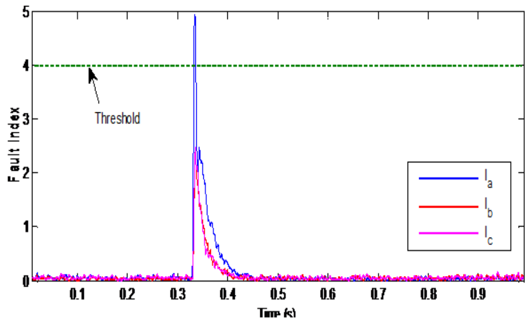

Fig. 17: Variation of Stockwell Transform-based fault index during the LG fault in the presence of WECS

B. Analysis of Double Line Fault

A LL fault is created by short-circuiting Phases A and B at Bus 838 in the presence of wind power generation. The corresponding three-phase current waveforms recorded at Bus 800 before and after fault occurrence are shown in Fig. 18. Following fault initiation, significant disturbances are observed in the currents of the faulted Phases A and B. Their current magnitudes initially increase considerably and subsequently decrease to values lower than the normal operating level. After the transient period, the currents gradually move toward their post-fault operating values. The healthy Phase C experiences comparatively smaller disturbances. These changes in the three-phase current waveforms clearly indicate the occurrence of an LL fault in the presence of WECS.

The corresponding variation of the proposed fault index for the three phases is presented in Fig. 19. The fault-index values of the faulted Phases A and B increase significantly and reach a maximum value of approximately 8.4, which is higher than the selected threshold value of 4. In contrast, the fault-index value of the healthy Phase C remains close to zero and below the threshold. Therefore, the proposed fault index successfully distinguishes the faulted Phases A and B from the healthy Phase C in the presence of wind power generation. The results further indicate that the proposed fault index responds rapidly after fault initiation, enabling timely identification of the LL fault under renewable energy penetration.

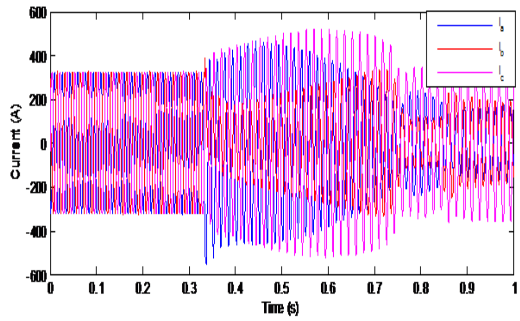

Fig. 18: Three-phase current waveforms during the LL fault in the presence of WECS

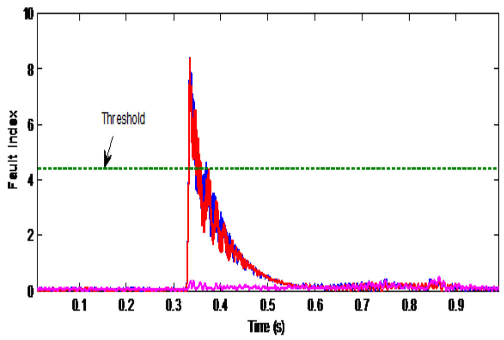

Fig. 19: Variation of the Stockwell Transform-based fault index during the LL fault in the presence of WECS

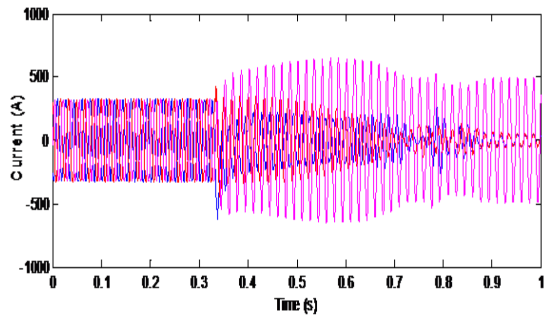

Fig. 20: Three-phase current waveforms during the LLG fault in the presence of WECS

C. Analysis of Double Line to Ground Fault

A double-line-to-ground (LLG) fault is created by simultaneously connecting Phases A and B to ground at Bus 838 in the presence of the wind energy conversion system. The corresponding three-phase current waveforms recorded at Bus 800 are presented in Fig. 20. The fault is initiated during the simulation, resulting in significant transient disturbances in the current waveforms. The magnitudes of the currents in the faulted Phases A and B change considerably following fault inception and subsequently decrease toward lower values. The current in the healthy Phase C also experiences a transient variation but gradually returns toward its normal operating condition. These waveform changes demonstrate the effect of the LLG fault on the distribution system with wind power generation.

The corresponding fault-index variations for all three phases are shown in Fig. 21. The fault-index values of the faulted Phases A and B increase significantly and reach approximately 9, which is well above the selected threshold value of 4. In comparison, the fault-index value of the healthy Phase C remains close to 2.5, which is below the threshold. Therefore, the proposed Stockwell Transform-based fault index effectively identifies the LLG fault and distinguishes the faulted Phases A and B from the healthy Phase C in the presence of wind power generation. The rapid increase in the fault index immediately after fault inception demonstrates the capability of the proposed method to detect the LLG fault within a short response time.

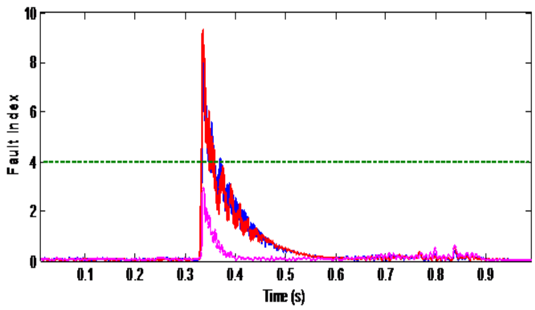

Fig. 21: Variation of the Stockwell Transform-based fault index during the LLG fault in the presence of WECS

D. Analysis of 3ϕ Fault Involving Ground

A three-phase-to-ground (LLLG) fault is created by simultaneously connecting Phases A, B, and C to ground at the test location in the presence of the WECS. The corresponding three-phase current waveforms recorded at Bus 800 are presented in Fig. 22. Before fault occurrence, the three-phase currents remain within their normal operating range. Following fault initiation, the current magnitudes of all three phases increase significantly, followed by a reduction toward lower values during the transient period. The considerable variation in the three-phase currents indicates the occurrence of a severe LLLG fault in the presence of wind power generation.

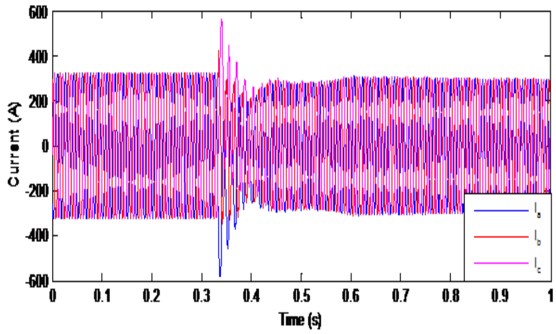

Fig. 22: Three-phase current waveforms during the LLLG fault in the presence of WECS

The corresponding variation of the proposed Stockwell Transform-based fault index is shown in Fig. 23. It is observed that the fault-index values of all three phases exceed the selected threshold value of 4. The maximum fault-index value reaches approximately 12 for one phase, while the values for the other two phases are approximately 8. Since the fault-index values of all three phases are higher than the threshold, the proposed algorithm successfully detects the occurrence of the LLLG fault and identifies the involvement of all three phases.

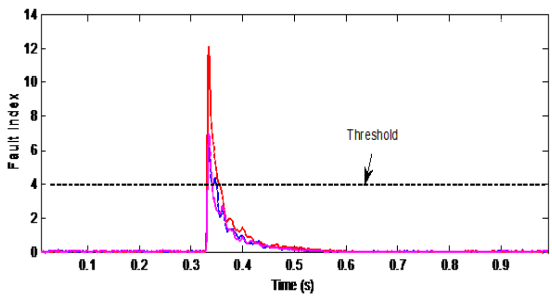

Fig. 23: Variation of the Stockwell Transform-based fault index during the LLLG fault in the presence of WECS

4.3.Comparative Analysis

The maximum fault-index values obtained for the different fault conditions in the presence of renewable energy generation are presented in Table 7. The results demonstrate that the proposed fault index can effectively distinguish among LG, LL, LLG, and LLLG faults based on the magnitude and distribution of the fault-index values across the three phases.

The LLLG fault produces the highest fault-index values, whereas the LG fault produces the lowest values. For the LL fault, the fault-index values of Phases A and B are approximately equal, while the index of the healthy Phase C is zero. In the case of the LLG fault, Phases A and B exhibit high fault-index values, whereas Phase C has a comparatively lower value. Thus, the proposed fault index can be used to distinguish between LL and LLG faults by examining the fault-index value of the third phase.

Table 7: Maximum Fault-Index Values for Different Fault Conditions in the Presence of Renewable Energy

S. No.	Type of fault	Phase-A	Phase-B	Phase-C
1	LG	5	2.5	2.5
2	LL	8.5	8.5	0
3	LLG	9	9	2.5
4	LLLG	12	8	8

Furthermore, the fault-detection elapsed time of the proposed Stockwell Transform (ST)-based method is compared with the NRHV-based method reported by Guillen et al. The comparison is presented in Table 8. The results show that the proposed ST-based approach requires less detection time for all the considered fault types. The detection time is 0.09 ms for LG, 0.257 ms for LL, 0.912 ms for LLG, and 0.098 ms for LLLG faults. The lower detection time indicates that the proposed ST-based method can identify faults rapidly and with a lower computational burden. Therefore, the proposed methodology demonstrates its effectiveness for fast fault detection in transmission systems with renewable energy penetration.

Table 8: Comparison of Fault-Detection Elapsed Time

S. No.	Fault Type	NRHV Method (ms)	ST Method (ms)
1	LG	1.118	0.09
2	LL	1.313	0.257
3	LLG	0.988	0.912
4	LLLG	1.118	0.098

ISSN 2277 – 8322

V. CONCLUSIONS

This research presented a fault detection and identification method based on the Stockwell Transform (ST) for power system networks with and without renewable energy integration. The proposed method uses the median value obtained from the S-matrix of the three-phase current signals to develop a fault index. The method was implemented and evaluated in MATLAB/Simulink using the IEEE-33 bus test system. In the absence of renewable energy sources, the proposed method successfully detected and identified different types of faults, including LG, LL, LLG and LLLG faults. The fault index values were used to distinguish the faulty phases from the healthy phases and to classify different fault types. The LLLG fault produced the highest fault index values, whereas the LG fault produced the lowest values. The LL and LLG faults showed similar fault index values in the faulty phases; however, their values in the healthy phase helped to distinguish between these two fault types.

The proposed method was also evaluated with a 1.5 MW wind energy conversion system integrated into the IEEE-33 bus network. The results demonstrated that the method remained effective in the presence of wind power generation and successfully detected LG, LL, LLG, and LLLG faults. The obtained fault indices clearly distinguished faulty phases from healthy phases. The comparative analysis also showed that the proposed Stockwell Transform-based method required less fault detection time than the considered conventional method, indicating its suitability for fast power system fault detection. Overall, the study demonstrates that the proposed Stockwell Transform-based fault index provides an effective and computationally efficient approach for detecting and identifying different types of power system faults under both conventional and renewable-energy-integrated operating conditions.

REFERENCES

[1] Y. Liu, X. He, Z. Wang, and D.-H. Zhou, “Fault detection and diagnosis for a class of nonlinear systems with decentralized event-triggered transmissions,” IFAC-PapersOnLine, pp. 1134–1139, 2015.

[2] Ch. D. Prasad and N. Srinivasu, “Fault detection in transmission lines using instantaneous power with ED based fault index,” Procedia Technology, vol. 21, pp. 132–138, 2015.

[3] V. H. Ferreira, R. Zanghi, M. Z. Fortes, G. G. Sotelo, R. B. M. Silva, J. C. S. Souza, C. H. C. Guimarães, and

ISSN 2277 – 8322

S. Gomes Jr., “A survey on intelligent system application to fault diagnosis in electric power system transmission lines,” Electric Power Systems Research, vol. 136, pp. 135–153, 2016.

[4] S. Hussain and A. H. Osman, “Fault location scheme for multi-terminal transmission lines using unsynchronized measurements,” International Journal of Electrical Power & Energy Systems, vol. 78, pp. 277–284, 2016.

[5] A. G. Shaik and R. R. V. Pulipaka, “A new wavelet based fault detection, classification and location in transmission lines,” International Journal of Electrical Power & Energy Systems, vol. 64, pp. 35–40, 2015.

[6] M. Dehghani, M. H. Khooban, and T. Niknam, “Fast fault detection and classification based on a combination of wavelet singular entropy theory and fuzzy logic in distribution lines in the presence of distributed generations,” International Journal of Electrical Power & Energy Systems, vol. 78, pp. 455–462, 2016.

[7] M. M. Rahman and A. K. Srivastava, “Detection, classification, and localization of faults and failures in photovoltaic arrays: A review, comparative analysis, and path forward,” Discover Energy, vol. 6, Art. no. 26, 2026.

[8] D. Sarathkumar, M. Srinivasan, A. A. Stonier, R. Samikannu, N. R. Dasari, and R. A. Antony, “A technical review on classification of various faults in smart grid systems,” IOP Conference Series: Materials Science and Engineering, vol. 1055, Art. no. 012152, pp. 1–12, 2021.

[9] A. Yadav and S. Goad, “A review on fault detection using different techniques in electric power system,” Journal of Electrical and Power System Engineering, vol. 7, no. 3, 2021.

[10] A. Saxena, S. Dubey, and H. K. Yadav, “Three phase transmission lines fault detection,” International Journal of Progressive Research in Engineering Management and Science, vol. 2, no. 5, pp. 233–238, May 2022.

[11] A. Z. Bertoletti, G. Cardoso Junior, A. P. de Morais, G. Marchesan, and J. C. do Prado, “Ground and phase fault classification for half-wavelength transmission lines relaying purposes,” International Journal of Electrical Power & Energy Systems, vol. 148, 2023.